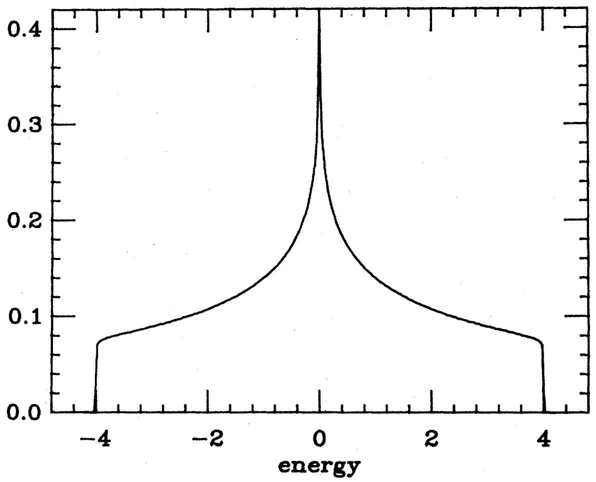

FIG. 2. Density of states for noninteracting electrons on a two-dimensional square lattice with nearest-neighbor hopping. The singularity at the origin is logarithmic.

The q-dependent zero-frequency susceptibility (per spin) for the noninteracting case is given by

$$\chi_0(q) = -\frac{1}{N}\sum_k \frac{f(\epsilon_{k+q}) - f(\epsilon_k)}{\epsilon_{k+q} - \epsilon_k} \tag{2.4}$$

with $f(\epsilon)$ the Fermi function:

$$f(\epsilon) = \frac{1}{e^{\beta\epsilon}+1} . \tag{2.5}$$

For $q=0$, we have

$$\chi_0(q=0) = \int d\epsilon\, g(\epsilon) \frac{\partial f}{\partial \epsilon} \xrightarrow[T\to 0]{} g(\epsilon_F) , \tag{2.6}$$

i.e., the usual Pauli result. In the half-filled case, the susceptibility diverges as $T \to 0$ due to the singularity in the density of states, as

$$\chi_0(q=0) \sim -\ln\left[\frac{T}{t}\right] . \tag{2.7}$$

The staggered susceptibility is given by

$$\begin{aligned}\chi_0(q=\pi) &= \frac{1}{N}\sum_k \frac{f(-\epsilon_k) - f(\epsilon_k)}{2\epsilon_k} \\ &= \int d\epsilon\, g(\epsilon) \frac{f(-\epsilon) - f(\epsilon)}{2\epsilon} .\end{aligned} \tag{2.8}$$

In the usual case where one has a nested Fermi surface this gives a logarithmic divergence of the susceptibility at low temperatures. Here, however, we have in addition the singularity in the density of states, and the low-temperature behavior in the half-filled case is

$$\chi_0(q=\pi) \sim \left[\ln\frac{T}{t}\right]^2 , \tag{2.9}$$

i.e., a stronger divergence than for the $q=0$ susceptibility. For the non-half-filled case, the q-dependent susceptibility is finite as $T \to 0$.

For nonzero U, the magnetic susceptibility within the random-phase approximation (RPA) is given by the sum of particle-hole ladder diagrams[18] as

$$\chi(q) = \frac{2\chi_0(q)}{1 - U\chi_0(q)} . \tag{2.10}$$

For the half-filled case, the divergences in χ_0 indicate instabilities for arbitrarily small values of U at both $q=0$ and $q=(\pi,\pi)$. Because the divergence in χ_0 is stronger for $q=(\pi,\pi)$, RPA predicts a transition to an antiferromagnetic phase at a higher temperature than for the ferromagnetic phase in the half-filled case. For the non-half-filled case, RPA predicts a transition at a *finite* value of U, since the susceptibility is nondivergent. The transition will be to states defined by the wave vector q for which χ_0 is maximum, which is a decreasing function of the band filling. However, because we are dealing with a two-dimensional model with a continuous symmetry, it is clear that no transition to a state with magnetic long-range order can occur expect possibly for $T=0$.

We now discuss the Hartree-Fock (HF) solution for this model. This has been discussed in detail by Penn for the three-dimensional case.[4] Within the Hartree-Fock approximation, the Hamiltonian is

$$\begin{aligned}H_{\mathrm{HF}} = &-t \sum_{\substack{\langle i,j\rangle \\ \sigma}} c_{i\sigma}^{\dagger} c_{j\sigma} \\ &+ U \sum_i \left(\langle n_{i\uparrow}\rangle n_{i\downarrow} + n_{i\uparrow}\langle n_{i\downarrow}\rangle - \langle n_{i\uparrow}\rangle\langle n_{i\downarrow}\rangle \right) \\ &-\mu \sum_i (n_{i\uparrow} + n_{i\downarrow}) .\end{aligned} \tag{2.11}$$

For the half-filled case, the appropriate solution is the antiferromagnetic one:

$$\begin{aligned}\langle n_{i\uparrow}\rangle &= n + (-1)^i m , \\ \langle n_{i\downarrow}\rangle &= n - (-1)^i m ,\end{aligned} \tag{2.12}$$

which yields the gap equation:

$$1 = \frac{U}{4\pi^2} \int d^2k \frac{1}{(\epsilon_k^2 + \Delta^2)^{1/2}} , \tag{2.13a}$$

$$\Delta = Um , \tag{2.13b}$$

which has a solution with $m \neq 0$ for arbitrarily small U due to the nesting of the Fermi surface. The features of the singularity are, however, different from the usual case. Rewriting Eq. (2.13a) as

$$1 = U \int_0^{4t} d\epsilon \frac{\rho(\epsilon)}{(\epsilon^2 + \Delta^2)^{1/2}} \tag{2.14}$$

and due to the singularity in the density of states, we find for the gap

$$\Delta \sim t e^{-2\pi\sqrt{t/U}} \quad (d=2) . \tag{2.15}$$

In contrast, both in one and three dimensions there is no singularity at the Fermi energy for the half-filled case, and the gap within HF behaves as

$$\Delta \sim te^{-2\pi t/U} \quad (d=1,3)\ . \tag{2.16}$$

This particular feature of the model under consideration gives a stronger tendency to antiferromagnetic ordering than in the usual case.[19] It should be remarked that the behavior, Eq. (2.15), is a consequence of the fact that both the nesting of the Fermi surface and the Van Hove singularity in the density of states occur at the same energy, the Fermi energy for the half-filled case. One can easily construct other band structures in $d=2$ where both features occur at different energies, or where the nesting is absent altogether, which will then have rather different properties. The logarithmic singularity, however, is required by topology in $d=2$ so that it always occurs. In the absence of nesting, it may give a tendency for ferromagnetic correlations.

For the non-half-filled band case we consider, in addition to (2.12), the possibility of ferromagnetic solutions:

$$\begin{aligned} \langle n_{i\uparrow}\rangle &= n+m\ , \\ \langle n_{i\downarrow}\rangle &= n-m\ , \end{aligned} \tag{2.17}$$

and paramagnetic ones, with $m=0$. The Hartree-Fock phase diagram, obtained by choosing the solution that gives the lowest energy (if more than one solution exists) is shown in Fig. 3, and is rather similar to the one obtained in $d=3$ by Penn. Note that for large U and fillings close to 1 ferromagnetism is predicted to occur. This is also in agreement with the exact results by Nagaoka,[20] who found the ferromagnetic state to be the ground state for $U=\infty$ and one hole in a half-filled-band system. However, we will see that our simulations do not give any indication that there is a tendency towards ferromagnetic ordering.

Finally, we review the strong-coupling limit of the model Eq. (2.1) for the half-filled-band case. To second order in the hopping the model is equivalent to an antiferromagnetic Heisenberg model, defined by the Hamiltonian

$$H_{\text{eff}} = +\frac{4t^2}{U}\sum_{\langle i,j\rangle} \mathbf{S}_i\cdot\mathbf{S}_j \tag{2.18}$$

with $\mathbf{S}$ the Pauli matrices. According to the finite lattice calculations of Oitmaa and Betts,[21] this model has antiferromagnetic long-range order in the ground state, approximately 50% reduced from the classical Néeel state due to quantum fluctuations. The existence of long-range antiferromagnetic order for the case $0<U<\infty$, where both spin and charge fluctuations occur, was an open question; in this work we believe we have established that the model indeed has antiferromagnetic order for $0<U<\infty$ in the half-filled-band case.

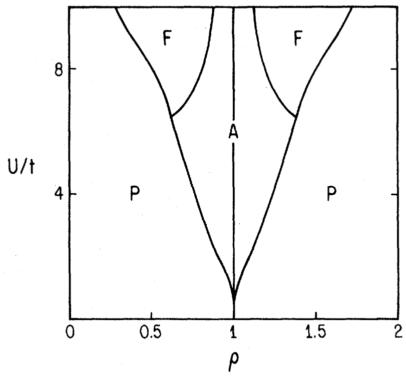

FIG. 3. Hartree-Fock phase diagram for the two-dimensional Hubbard model. A, F, and P denote antiferromagnetic, ferromagnetic, and paramagnetic ground states, respectively.

The behavior of the magnetic susceptibility at low temperatures in the limit where Eq. (2.18) is valid follows from a spin-wave analysis. Assuming a linear dispersion relation for the spin-wave energy, $\epsilon(k)\sim ck$, we obtain

$$\chi \sim \frac{1}{T}\int k dk \frac{e^{\beta k}}{(e^{\beta k}-1)^2} \sim T\ln T \tag{2.19}$$

at low temperatures. The staggered susceptibility should be the same as the susceptibility for a ferromagnet, with $\epsilon(k)\sim ck^2$, and yields

$$\chi(q=2k_F)\sim \frac{1}{T}\ , \tag{2.20}$$

which happens to be the same as the Curie law because we are in two dimensions. Note that the susceptibility in the large-U limit vanishes as $T\rightarrow 0$ [Eq. (2.19)], in contrast to the $U=0$ limit where it diverges [Eq. (2.7)].

III. THE SIMULATION

The simulation was constructed using an Ising functional integral formulation recently introduced. The partition function is written as

$$Z=\text{Tr}e^{-\beta H}=\text{Tr}\prod_{l=1}^{L} e^{-\Delta\tau H} \cong \text{Tr}\prod_{l=1}^{L} e^{-\Delta\tau H_0}\exp\left[-\Delta\tau\left[U\sum n_{i\uparrow}n_{i\downarrow}-\mu\sum(n_{i\uparrow}+n_{i\downarrow})\right]\right] \tag{3.1}$$

with H_0 the kinetic energy and $\beta=L\Delta\tau$. The error in the breakup in Eq. (3.1) is of order $O(\Delta\tau^2 tU)$. The electron-electron interaction was eliminated using the identity[14]

$$e^{-\Delta\tau U n_{i\uparrow}n_{i\downarrow}} = \text{Tr}_\sigma \exp\left[\lambda\sigma(n_{i\uparrow}-n_{i\downarrow})-\frac{\Delta\tau U}{2}(n_{i\uparrow}+n_{i\downarrow})\right] \tag{3.2}$$

with

$$\lambda = 2\arctan\sqrt{\tanh(\Delta\tau U/4)} \tag{3.3}$$

and $\sigma=\pm 1$. The partition function is then

$$\begin{aligned} Z&=\mathrm{Tr}_\sigma \mathrm{Tr} \prod_{l=1}^{L} e^{-\Delta\tau H_0} \exp\left[\lambda\sigma(n_{i\uparrow}-n_{i\downarrow})-\Delta\tau(\mu-U/2)(n_{i\uparrow}+n_{i\downarrow})\right] \\ &=\mathrm{Tr}_\sigma \mathrm{Tr}\left[\prod_{l=1}^{L} e^{-\Delta\tau H_{0\uparrow}} \exp\{[\lambda\sigma-\Delta\tau(\mu-U/2)]n_{i\uparrow}\}\right]\left[\prod_{l=1}^{L} e^{-\Delta\tau H_{0\downarrow}} \exp\{[-\lambda\sigma-\Delta\tau(\mu-U/2)]n_{i\downarrow}\}\right] . \end{aligned} \tag{3.4}$$

Denote

$$B_l(\alpha)=e^{-\Delta\tau K} e^{V^\alpha(l)} , \tag{3.5}$$

$$(K)_{ij}=\begin{cases} -t & \text{for } i,j \text{ nearest neighbors,} \\ 0 & \text{otherwise ,} \end{cases} \tag{3.6a}$$

$$V_{ij}^\alpha(l)=\delta_{ij}[\lambda\alpha\sigma_i(l)-\Delta\tau(\mu-U/2)] , \tag{3.6b}$$

and define the operators

$$D_l(\alpha)=e^{-\Delta\tau c_i^\dagger K_{ij} c_j} e^{c_i^\dagger V_i^\alpha(l) c_i} , \tag{3.7}$$

so that the partition function is

$$Z=\mathrm{Tr}_\sigma \mathrm{Tr} \prod_{\alpha=\pm 1} \prod_{l=1}^{L} D_l(\alpha) . \tag{3.8}$$

We can take the trace over fermions explicitly, since there are only bilinear forms in fermion operators, and obtain

$$\begin{aligned} Z&=\mathrm{Tr}_\sigma \prod_\alpha \det[1+B_L(\alpha)B_{L-1}(\alpha)\cdots B_1(\alpha)] \\ &\equiv \mathrm{Tr}_\sigma \det O_\uparrow \det O_\downarrow . \end{aligned} \tag{3.9}$$

This identity was proved by Blankenbecler *et al.*,[15] using Grassmann variables. For the reader unfamiliar with Grassmann algebras, we give an elementary derivation of this result in the Appendix.

The remaining sum over Ising spins in Eq. (3.9) is performed using a Monte Carlo technique, taking as Boltzmann weight the product of determinants in Eq. (3.9). For the case of a half-filled band, it is easy to show that this product is positive for arbitrary σ configurations. Consider the particle-hole transformation

$$\begin{aligned} d_{i\sigma}&=(-1)^i c_{i\sigma}^\dagger , \\ c_{i\sigma}^\dagger c_{i\sigma}&=1-d_{i\sigma}^\dagger d_{i\sigma} . \end{aligned} \tag{3.10}$$

For the half-filled band, $\mu=U/2$ and we have from Eq. (3.4)

$$\begin{aligned} \det O_\uparrow&=\mathrm{Tr}_c \prod_{i=1}^{L} e^{-\Delta\tau H_{0\uparrow}} e^{\lambda\sigma c_{i\uparrow}^\dagger c_{i\downarrow}} \\ &=\mathrm{Tr}_d \prod_{i=1}^{L} e^{-\Delta\tau H_{0\uparrow}} e^{-\lambda\sigma d_{i\uparrow}^\dagger d_{i\downarrow}} e^{\lambda\sigma_i(l)} , \end{aligned} \tag{3.11}$$

so that

$$\det O_\uparrow=e^{\lambda\sum_{i,l}\sigma_k(l)} \det O_\downarrow \tag{3.12}$$

and the product of determinants in Eq. (3.9) is positive definite, so that it can be used as a Boltzmann weight. For the non-half-filled band, we define the Boltzmann weight as

$$P(\sigma)=|\det O_\uparrow \det O_\downarrow| \tag{3.13}$$

and have to compute the average sign of the product of determinants. We find that the product of determinants does become negative for certain field configurations, but the average sign is always well behaved and does not go to zero rapidly as β or the lattice size increases, so that it does not represent a problem for doing Monte Carlo simulations.

We use the heat-bath algorithm to perform the sum over Ising spins. If R_α is the ratio of the new to the old determinant for fermion spin α on flipping a given Ising spin, it is flipped with probability

$$P=\frac{R_\uparrow R_\downarrow}{1+R_\uparrow R_\downarrow} . \tag{3.14}$$

To compute R_α, we use the procedure introduced by Blankenbecler, Scalapino, and Sugar[15] which involves updating the full Green's function exactly when a move is accepted. This takes the bulk of the computer time in the calculation, N^2 operations per update, with N the number of spatial sites. After several updatings, the Green's function degrades due to rounding errors and has to be recomputed from scratch. This makes a non-negligible difference in terms of computer time only if it has to be done every time slice or two. In practice, we started our simulations by recomputing G from scratch every 10 time slices and checking whether it had degraded by more than 1%. If so, we recomputed it more often, which we had to do for large values of the interaction.

We now consider the evaluation of average quantities. First, it is easy to show that[14]

$$\begin{aligned} &\langle (n_{i\uparrow}(\tau)-n_{i\downarrow}(\tau))(n_{j\uparrow}(0)-n_{j\downarrow}(0))\rangle \\ &\qquad=(1-e^{-\Delta\tau U})^{-1}\langle \sigma_i(\tau)\sigma_j(0)\rangle , \end{aligned} \tag{3.15}$$

so that we obtain fermion spin-spin correlation functions simply from correlation functions of the Ising spins. For other correlation functions, we do not have enough information in the Ising variables but have to average over appropriate fermion matrices. For an equal time correlation of the operators P_i and Q_j we have

$$\begin{aligned} \langle\langle P_i Q_j \rangle\rangle&=\frac{\mathrm{Tr}_\sigma \mathrm{Tr} P_i Q_j \prod_\alpha \prod_l D_l(\alpha)}{Z} \\ &=\frac{\mathrm{Tr}_\sigma \langle P_i Q_j \rangle \det O_\uparrow \det O_\downarrow}{Z} , \end{aligned} \tag{3.16}$$

$$\langle P_i Q_j \rangle=\frac{\mathrm{Tr} P_i Q_j \prod_{l,\alpha} D_l(\alpha)}{\det O^\uparrow \det O_\downarrow} . \tag{3.17}$$

It is easy to obtain the appropriate formulas by using the transformation to normal modes, Eq. (A6), of the entire product of factors in (3.17). For example, consider the single-particle Green's functions (we omit spin indices for simplicity):

$$\langle c_i c_j^\dagger \rangle = \frac{\mathrm{Tr}\, c_i c_j^\dagger \prod_\nu e^{-c_\nu^\dagger l_\nu c_\nu}}{\prod_\nu (1+e^{-l_\nu})}$$

$$= \sum_{\nu'} \langle \nu' | i \rangle \langle j | \nu' \rangle \frac{\mathrm{Tr}\, c_{\nu'} c_{\nu'}^\dagger \prod_\nu e^{-c_\nu^\dagger l_\nu c_\nu}}{\prod_\nu (1+e^{-l_\nu})}$$

$$= \sum_{\nu'} \langle \nu' | i \rangle \langle j | \nu' \rangle \frac{1}{1+e^{-l_{\nu'}}}$$

$$= \left[\frac{1}{1+B_L B_{L-1} \cdots B_1} \right]_{ij} . \tag{3.18}$$

Similarly,

$$\langle c_i^\dagger c_j \rangle = \left[B_L \cdots B_1 \frac{1}{1+B_L \cdots B_1} \right]_{ji} . \tag{3.19}$$

For two-particle Green's functions, it is straightforward to show, by expanding in eigenstates, that Wick's theorem applies, i.e.,

$$\langle c_{i_1}^\dagger c_{i_2} c_{i_3}^\dagger c_{i_4} \rangle = \langle c_{i_1}^\dagger c_{i_2} \rangle \langle c_{i_3}^\dagger c_{i_4} \rangle + \langle c_{i_1}^\dagger c_{i_4} \rangle \langle c_{i_2} c_{i_3}^\dagger \rangle . \tag{3.20}$$

Note that this decoupling applies only to the "single-bracket" average (trace over fermions) and not to the full average, denoted by double angular brackets [Eq. (3.16)], which involves the additional trace over spins. For averages involving fermion operators of both spins we can simply factorize, since everything is diagonal in spins, for example,

$$\langle n_{i\uparrow} n_{j\downarrow} \rangle = \langle n_{i\uparrow} \rangle \langle n_{j\downarrow} \rangle . \tag{3.21}$$

Finally, we can obtain in a similar fashion time-dependent correlation functions, by inserting the operators at different points in the product over time slices Eq. (3.8). For example, a time-dependent Green's function is

$$\begin{aligned} \langle c_i(l_1) c_j^\dagger(l_2) \rangle &= \frac{\mathrm{Tr} D_L D_{L-1} \cdots D_{l_1+1} c_i D_{l_1} \cdots D_{l_2+1} c_j^\dagger D_{l_2} \cdots D_1}{\mathrm{Tr} D_L \cdots D_1} \\ &= \frac{\mathrm{Tr} D_{l_2} \cdots D_1 D_L \cdots D_{l_2+1} [(D_{l_1} D_{l_1-1} \cdots D_{l_2+1})^{-1} c_i D_{l_1} \cdots D_{l_2+1}] c_j^\dagger}{\mathrm{Tr} D_{l_2} \cdots D_1 D_l \cdots D_{l_2+1}} . \end{aligned} \tag{3.22}$$

By expanding in eigenstates of $D_{l_1} D_{l_1-1} \cdots D_{l_2+1}$, we find

$$(D_{l_1} D_{l_1-1} \cdots D_{l_2+1})^{-1} c_i D_{l_1} D_{l_1-1} \cdots D_{l_2+1} = \sum_k (B_{l_1} B_{l_1-1} \cdots B_{l_2+1})_{ik} c_k , \tag{3.23}$$

and replacing in (3.22)

$$\langle c_i(l_1) c_j^\dagger(l_2) \rangle = \sum_k (B_{l_1} B_{l_1-1} \cdots B_{l_2+1})_{ik} \frac{\mathrm{Tr} D_{l_2} \cdots D_1 D_L \cdots D_{l_2+1} c_k c_j^\dagger}{\mathrm{Tr} D_{l_2} \cdots D_1 D_l \cdots D_{l_2+1}} \tag{3.24}$$

and using (3.18), we finally obtain

$$\langle c_i(l_1) c_j^\dagger(l_2) \rangle = \left[B_{l_1} B_{l_1-1} \cdots B_{l_2+1} \frac{1}{1+B_{l_2} \cdots B_1 B_L \cdots B_{l_2+1}} \right]_{ij} . \tag{3.25}$$

Similarly,

$$\langle c_i^\dagger(l_1) c_j(l_2) \rangle = \left[\frac{1}{1+B_{l_2} \cdots B_{l_2+1}} B_{l_2} \cdots B_{l_1+1} \right]_{ij} , \tag{3.26}$$

and for higher-order correlation functions Wick's theorem applies. From these formulas we can obtain arbitrary correlation functions of interest in the Hubbard model, such as charge and spin correlation functions and susceptibilities.

We have done a variety of checks on our simulation program to make sure it was running properly. For the noninteracting case our results should be exact for a finite lattice, and we have verified this by comparing the results from our simulation program with those obtained from a direct calculation for lattices up to 8×8 in spatial size and various temperatures. For the interacting case, we have earlier reported comparison with exact results for two sites,[14] where we found that the choice $\Delta\tau U = 0.5$ gives reasonable accuracy (within a few percent). In Figs. 4 and 5 we show comparison of our simulation results for the local moment [Eq. (4.1)] and the magnetic susceptibility [Eq. (4.2)] for 6-site rings with the exact results of Shiba.[7] It can be seen that the agreement is excellent. These tests lead us to believe that the results to be presented in the next section for the two-dimensional Hubbard model are reliable.

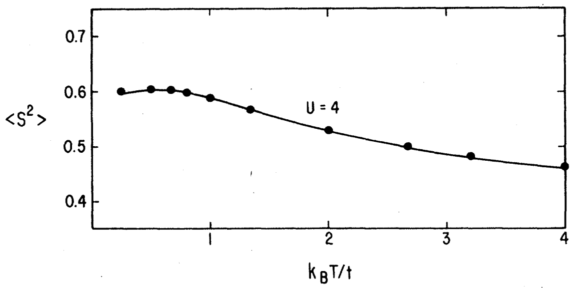

FIG. 4. Local moment versus temperature for a 6-site ring, $U=4$, with $\Delta\tau=0.125$. The solid line is the exact result of Shiba.

IV. RESULTS FOR THE HALF-FILLED-BAND CASE

We have performed simulations in the half-filled-band sector for lattices up to 8×8 in spatial size (with periodic boundary conditions) and interaction strengths $U=2$, 4, and 8. The time slice size was taken to be $\Delta\tau=0.25$, 0.125, and 0.0625 for $U=2$, 4, and 8, respectively. Simulations were performed on a Vax 750 computer and a Cray 1S supercomputer. A sweep through a 6×6 lattice with 32 time slices took 70 sec on the Vax and 0.60 sec on the Cray, plus some fraction of this number depending on the measurements performed. Typically, 200 warm-up and 1000 measurements separated by two sweeps were performed for a given set of parameters. For low temperatures, the algorithm becomes unstable, and the lowest temperature we could study without running into accuracy problems was $\beta=4$ on the Cray (using single precision) and $\beta=4.5$ on the Vax (using double precision). Our program on the Cray with double precision was a factor of 15 to 20 slower so that it was impractical. Because more time slices are needed the larger the interaction and the algorithm becomes unstable more rapidly, we could not reach as low temperatures with $U=8$ as with $U=2$. Also, the statistical error becomes larger the larger the interaction.

Figure 6 shows the local magnetic moment, defined by

$$\langle S^2\rangle = \tfrac{1}{4}\langle \sigma_x^2+\sigma_y^2+\sigma_z^2\rangle = \tfrac{3}{4}\langle \sigma_z^2\rangle \ , \tag{4.1a}$$

$$\sigma_z^i = n_{i\uparrow} - n_{i\downarrow} \ . \tag{4.1b}$$

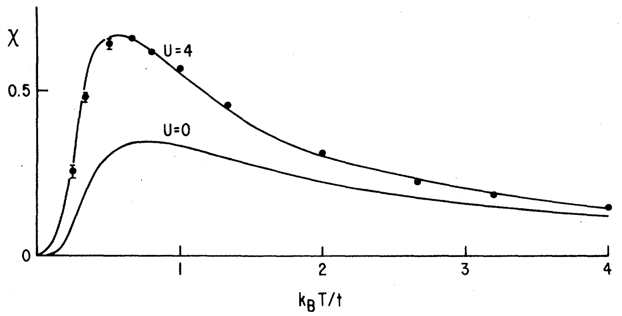

FIG. 5. Magnetic susceptibility versus temperature for a 6-site ring, $U=4$, with $\Delta\tau=0.125$. The solid line is the exact result of Shiba.

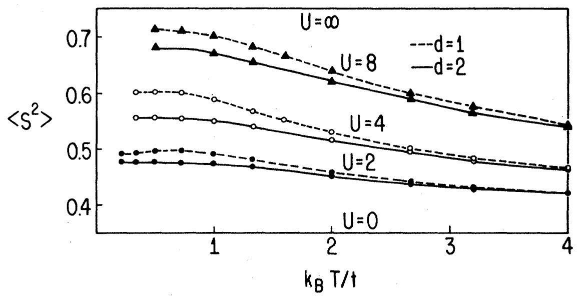

FIG. 6. Local magnetic moment versus temperature on a 6×6 two-dimensional lattice and a 6-site one-dimensional lattice.

The local moment increases gradually as the temperature is lowered, indicating that the electrons are becoming more localized. There is no evidence of any abrupt change as a function of temperature. It also increases gradually as a function of U, and for $U=8$ (equals bandwidth) it is already quite close to the $U=\infty$ value at low temperatures. We also show results for the one-dimensional case for comparison. In units of the bandwidth, the Hubbard interaction is more effective in localizing the electrons as the dimensionality increases.

Figure 7 shows the magnetic susceptibility versus tem-

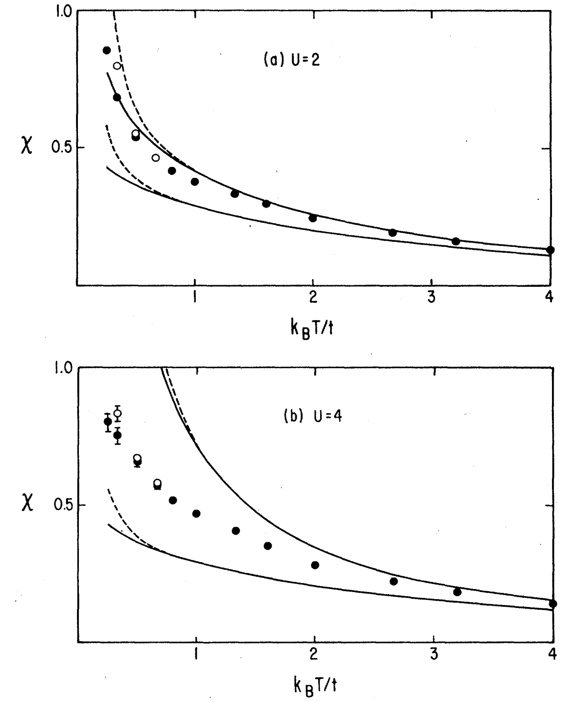

FIG. 7. Magnetic susceptibility versus temperature. The solid circles (open circles) are Monte Carlo results for a 6×6 (4×4) lattice. The lower solid line is the noninteracting result for an infinite lattice, the upper solid line the RPA prediction. The dashed line is the corresponding result for a 6×6 lattice, showing that finite-size effects start to appear around $T\sim 0.75$. For the interacting case, finite-size effects appear at a somewhat lower temperature.

perature for $U=2$ and 4. Some results for $U=8$ were given in Ref. 16. The q-dependent (zero-frequency) susceptibility is defined by

$$\chi(q)=\frac{1}{N}\sum_{i,j} e^{iq(R_i-R_j)}\int_0^\beta d\tau\langle[n_{i\uparrow}(\tau)-n_{i\downarrow}(\tau)]\times[n_{j\uparrow}(0)-n_{j\downarrow}(0)]\rangle \quad (4.2)$$

and for $q=0$ it satisfies

$$\chi(q=0)=\beta S(q=0) \quad (4.3)$$

with $S(q)$ the magnetic structure factor,

$$S(q)=\frac{1}{N}\sum_{i,j} e^{iq(R_i-R_j)}\langle(n_{i\uparrow}-n_{i\downarrow})(n_{j\uparrow}-n_{j\downarrow})\rangle\ , \quad (4.4)$$

since the total magnetization commutes with the Hamiltonian. We evaluated the susceptibility using both sides of Eq. (4.3) and found agreement within statistical error. The susceptibility increases smoothly as the temperature is lowered, and there is a slight bulge (particularly for $U=4$) for T between 1 and 2, which is where the local moment is increasing more rapidly. As $T\rightarrow 0$, χ diverges logarithmically if $U=0$ [Eq. (2.7)] because of the logarithmic singularity in the density of states, and we expect it to go to zero for large U [Eq. (2.19)]. Although we do not see this behavior up to the lowest temperature studied, χ does increase less rapidly for $U=4$ than for $U=2$ at low temperatures. Except at the lowest temperatures, where the singularity in $\rho(\epsilon)$ plays a role, χ is enhanced more the larger U is, as one would expect. We also show in Fig. 7 the RPA results, Eq. (2.10). From comparison with the Monte Carlo results, we conclude that RPA is fairly accurate for $U=2$, but becomes rapidly inaccurate as U is increased, and it always predicts too large an enhancement of the susceptibility.

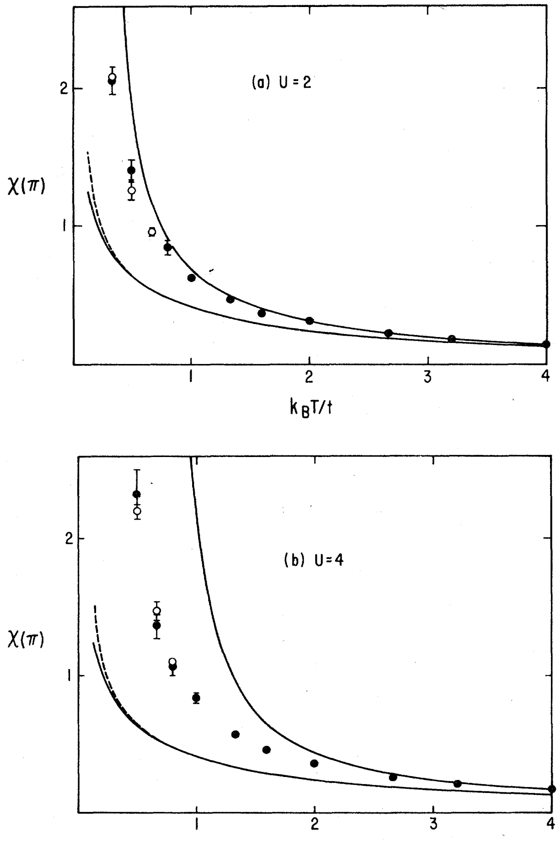

FIG. 8. Same as Fig. 7 for the staggered magnetic susceptibility.

Figure 8 shows the staggered magnetic susceptibility versus temperature. Here, for the free case we have the combined effect of the singularity in the density of states and the nested Fermi surface, yielding a low-temperature behavior $\chi_{st}\sim\ln^2(T/t)$. For large U, we expect $\chi_{st}\sim 1/T$ at low temperatures, as discussed in Sec. II. Our results for finite U appear to follow the stronger divergence $\chi_{st}\sim 1/T$. Similarly, as for the susceptibility, RPA overestimates the effect of the interaction, but it is quite accurate for $U=2$ in the temperature range studied. However, RPA predicts a transition to an antiferromagnetic state at $T=0.33$ and 0.75 for $U=2$ and 4, respectively, and we find no evidence for it, as one would expect.

Figure 9 shows the internal energy versus temperature. It is a smoothly varying function of temperature and increases as U is increased. We have extrapolated the ground-state energy assuming a T^2 dependence at low temperature and using our Monte Carlo data for the lowest temperatures. The extrapolated results are $E=-1.17(2)$ for $U=2$, $E=-0.88(3)$ for $U=4$, and $E=-0.48(5)$ for $U=8$. The errors are estimates on the error due to the extrapolation, since the statistical error is very small. The extrapolated data are shown in the inset, where they are compared with results from the Hartree-Fock approximation and an exact lower bound obtained

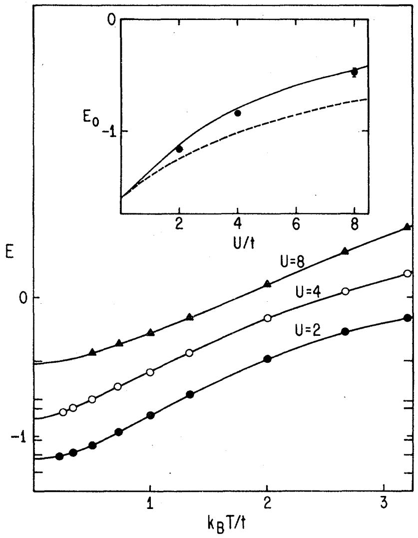

FIG. 9. Energy versus temperature for $U=2$, 4, and 8. The inset shows the extrapolated ground-state energy, compared with Hartree-Fock predictions (solid line) and the Langer-Mattis lower bound (dashed line).

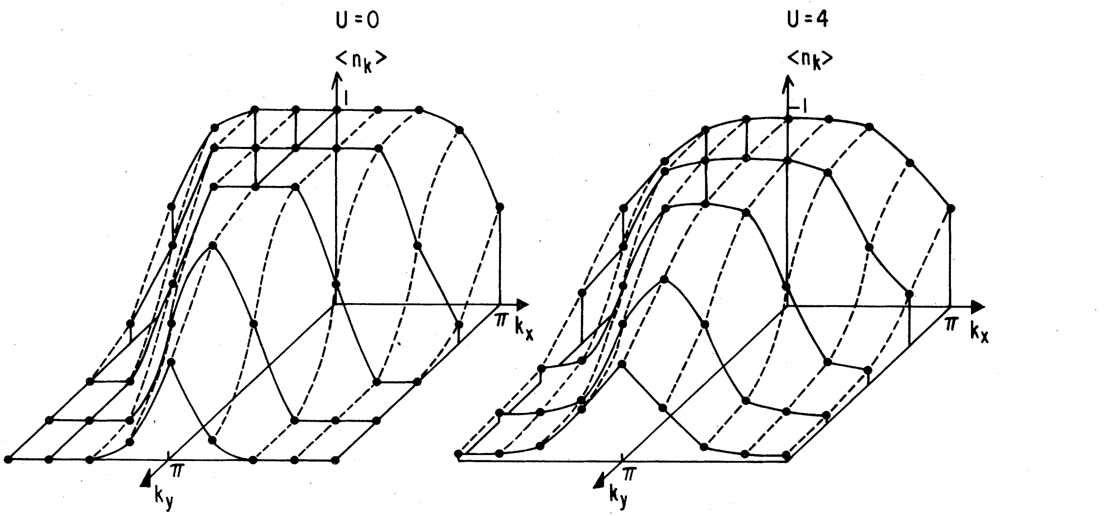

FIG. 16. Occupation number in k space, $n_k = \langle c_k^\dagger c_k \rangle$ on an 8×8 lattice at $\beta=4$. Note how the interaction causes a rounding, and even at $k=0$ the occupation number is less than unity due to the electron-electron interaction.

It is not possible to determine from such a small system whether a well-defined Fermi surface still exists. It is believed, however, from general arguments, that the Fermi surface is destroyed for $U\neq0$, since the system becomes an insulator.

V. NON-HALF-FILLED BAND

We have performed simulations for band fillings other than one-half for $U=4$ and $U=8$. As mentioned in Sec. III, the determinant does become negative for some cases if the band is not half-full, and it becomes necessary to compute the average sign. This happens particularly for large values of the interaction. Table I shows some results for the average sign for various cases. It can be seen that the average sign does become somewhat smaller as the temperature decreases, and does not seem to be very dependent on lattice size. As a function of band filling, it first decreases and then increases again as the band filling is further decreased. For the parameter range studied, the average sign did not become small enough to cause problems in the simulations. It is not clear whether as $\beta\to\infty$ the average sign vanishes, and if so how. It certainly does not appear to be vanishing exponentially, as in methods where the fermions are not integrated out, but could possibly be vanishing algebraically.

Figure 17 shows the behavior of the spin-spin correlation functions for $U=4$ and several band fillings, for 6×6 lattices at $\beta=4.5$. We also show the results for 4×4, $\beta=3$. Except for the case $\rho=1$, there is essentially no change in the spin-spin correlations in going to larger lattices and decreasing the temperature. This suggests that there is no magnetic order except for $\rho=1$. The peak value shifts from (π,π) as the filling is decreased. The results are very similar to the ones obtained with no correlations except for the $\rho=1$ case.

Figure 18 shows the case $\rho=0.9$ for 4×4 at $\beta=2$; 6×6, $\beta=3$; and 8×8, $\beta=4$. The peak is still at (π,π) here, since we are close to the half-filled band, and there is a small increment in going to larger lattices and increasing β. There is a large difference, however, with the cor-

TABLE I. Average value of the sign of the product of determinants for some cases where the band is non-half-filled. For the half-filled case, the sign is always positive.

U	Band filling	Lattice size	β	$\langle$Sign$\rangle$
4	0.9	4×4	2	1
			3	0.99
			4	0.94
		8×8	4	0.93
	0.84	4×4	3	0.99
		6×6	4.5	0.77
	0.65	4×4	3	0.99
		6×6	4.5	0.97
	0.48	4×4	3	1
		6×6	4.5	1
8	0.67	4×4	2	0.98
		6×6	3	0.61

TABLE II. On-site and nearest-neighbor spin-spin correlations for $U=8$, $\beta=3$ on a 4×4 lattice for various band fillings. $i+\delta$ denotes a nearest neighbor of site i. The number in parentheses is the statistical error in the last figure.

Band filling	$\langle\sigma_z^2\rangle$	$\langle\sigma_{z,i}\sigma_{z,i+\delta}\rangle$
1	0.899(3)	−0.31(4)
0.91	0.841(4)	−0.21(3)
0.81	0.750(2)	−0.12(4)
0.67	0.636(2)	−0.089(2)
0.60	0.565(2)	−0.079(5)
0.42	0.400(8)	−0.036(7)
0.25	0.247(6)	−0.017(2)

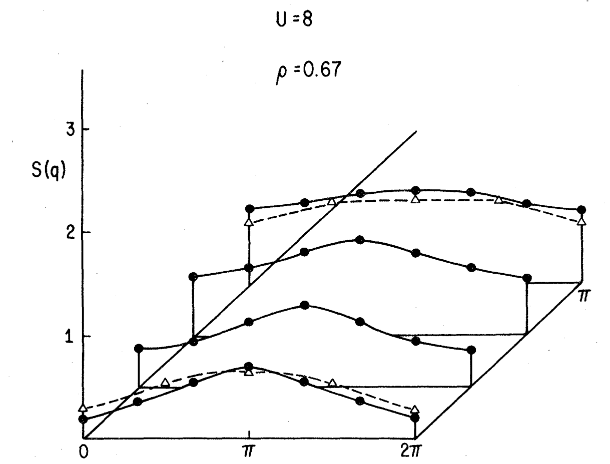

FIG. 20. Magnetic structure factor for $U=8$, $\rho=0.67$ on a 6×6 lattice, $\beta=3$, and a 4×4 lattice, $\beta=2$. Note that there is no indication of ferromagnetism, in contradiction with HF theory.

$S(\pi,\pi)/N$ versus $1/N$ for this case. Although not quite unambiguous, the results suggest that the system does not have antiferromagnetic order in the thermodynamic limit.

We now consider a case which according to mean-field theory should have a ferromagnetic ground state: $U=8$, $\rho=0.65$. The spin-spin correlations in real space show no evidence of even short-ranged ferromagnetic correlations, but rather weak antiferromagnetic correlations. The structure factor is shown in Fig. 20. It has a broad peak at (π,π) but rather weak dependence on lattice size and temperature, suggesting that there is no long-range order here either. In fact, the $q=0$ structure factor *decreases* as the temperature is lowered. We have also explored other band fillings for $U=8$, and found nowhere even short-ranged ferromagnetic correlations. Table II shows the on-site and nearest-neighbor correlations for $U=8$ and several band fillings. It can be seen that the nearest-neighbor correlations are always antiferromagnetic, becoming weaker as the band filling decreases. We conclude that the system shows no tendency for ferromagnetic correlations in the parameter range studied.

Finally, we have also studied pairing correlations in our simulation. We measured the singlet- and triplet-pairing susceptibility, given by

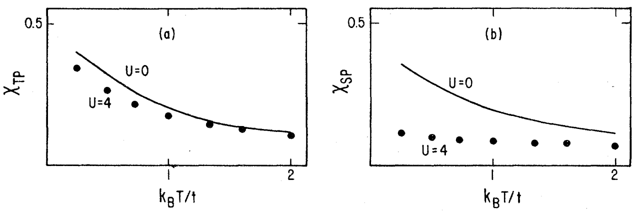

FIG. 21. (a) Triplet- and (b) singlet-pairing susceptibility at $q=0$ versus temperature for $U=0$ and $U=4$, $\rho\sim0.65$.

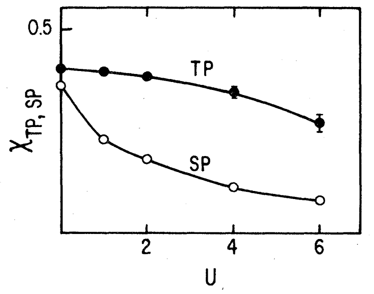

FIG. 22. Triplet- and singlet-pairing susceptibilities at $q=0$ versus U for $\beta=4$, $\rho\sim0.65$.

$$\chi_{SP}(q)=\frac{1}{N}\sum_{i,j} e^{iq(R_i-R_j)}\int_0^\beta d\tau\langle c_{i\uparrow}(\tau)c_{i\downarrow}(\tau)c_{j\downarrow}^\dagger(0)c_{j\uparrow}^\dagger(0)\rangle\ , \qquad (5.1)$$

$$\chi_{TP}(q)=\frac{1}{N}\sum_{i,j} e^{iq(R_i-R_j)} \times\int_0^\beta d\tau\langle c_{i\uparrow}(\tau)c_{i+\hat{x},\uparrow}(\tau)c_{j+\hat{x},\uparrow}^\dagger(0)c_{j\uparrow}^\dagger(0)\rangle\ . \qquad (5.2)$$

These susceptibilities peak at $q=0$, and diverge if the system undergoes a transition to a singlet or triplet superconducting state. Figure 21 shows the temperature dependence of $\chi_{TP}(q=0)$ and $\chi_{SP}(q=0)$ for $U=0$ and $U=4$, and band filling $\rho\sim0.65$. χ_{SP} is strongly suppressed by U, as one would expect. χ_{TP} for $U=4$ appears to grow in a similar way as for the noninteracting case (χ_{TP} at $U=0$ diverges logarithmically as $T\rightarrow0$), but it is smaller at all temperatures. Figure 22 shows the dependence of the triplet- and singlet-pairing susceptibilities on U for $\rho\sim0.65$ at a fixed low temperature; both susceptibilities are suppressed with U, although χ_{SP} much more rapidly. We find also that the suppression is larger for the band closer to half-full. We have also measured the triplet-pairing susceptibility for antiparallel spins, and obtained results very close to χ_{TP}.

Our results for χ_{TP} are surprising, since it has been argued that spin fluctuations should give rise to triplet pairing in a model with strong short-ranged repulsive interactions like the Hubbard model;[26] in particular, it is believed that in ^{3}He the short-ranged repulsion is the dominant mechanism causing superfluidity.[26] Our findings cast doubt on this picture, at least in two dimensions. For the ^{3}He case, we believe that the longer-range attractive tail in the potential is crucial, and simulations on a Hubbard model with nearest-neighbor attractive interactions are in progress.

VI. THE ATTRACTIVE HUBBARD MODEL

We now discuss briefly the properties of the attractive Hubbard model in the half-filled-band case. We can do this without extra work, since as is well known, a particle-hole transformation can map $U>0$ into $U<0$. The transformation is[27]

$$d_{i\uparrow}=c_{i\uparrow}\,,\qquad d_{i\downarrow}=c_{i\downarrow}^{\dagger}(-1)^{i}\,, \tag{6.1}$$

which takes $U\rightarrow -U$ and leaves the kinetic energy invariant. Under this transformation, S_z-S_z correlations are mapped onto charge-density correlations:

$$n_{i\uparrow}-n_{i\downarrow}\rightarrow n_{i\uparrow}+n_{i\downarrow}\,, \tag{6.2}$$

so that long-range antiferromagnetic order corresponds to a charge-density-wave (CDW) state. We have also, however, long-range antiferromagnetic order in the other directions of spin space; the spin operator in the x direction, for example, is

$$S_x^i=c_{i\uparrow}^{\dagger}c_{i\downarrow}+c_{i\downarrow}^{\dagger}c_{i\uparrow}\rightarrow d_{i\uparrow}^{\dagger}d_{i\downarrow}^{\dagger}+d_{i\downarrow}d_{i\uparrow}\,, \tag{6.3}$$

and long-range order in the x component of the spin corresponds to long-range singlet superconducting order in the attractive case. We conclude then that the ground state of the two-dimensional attractive Hubbard model (half-filled) is very peculiar in that it exhibits simultaneously CDW and superconducting long-range order. In the presence of any small perturbation, for example, a longer-range electron-electron interaction, one of the types of order will probably be destroyed and the other further stabilized. This is an interesting question to explore further.

VII. CONCLUSIONS

We have studied properties of the two-dimensional Hubbard model on a square lattice using Monte Carlo simulations. As mentioned in Sec. II, we expect some of the features found here to be very specific to the model studied and others to be more general. The purpose of this study was to provide answers to the following questions. (a) What are the properties of the simplest lattice model of interacting electrons in two dimensions? (b) How useful is the Hubbard model to describe electron correlations and its consequences for narrow-band systems? And, (c) how well does mean-field theory describe the model? We believe we have provided at least partial answers to these questions. Finally, another purpose of our work was to demonstrate that numerical simulations can be a useful tool to study interacting electron systems in more than one dimension.[28]

Our conclusions can be summarized by the phase diagram in Fig. 23. We have shown that for the half-filled band case the system exhibits antiferromagnetic long-range order for all values of the interactions. This conclusion is by no means obvious: In the $U=\infty$ limit, spin fluctuations reduce the long-range order to 50% of its classical value, as shown by Betts and Oitmaa; one might have expected that for any $U<\infty$, charge fluctuations destroy the order altogether, or that a critical value U_c exists below which no long-range order exists. Even though the susceptibility diverges for $U=0$, this does not prove that long-range order exists for any $U>0$; recall the case of one-dimensional spinless fermions with a nearest-neighbor repulsion V, where, even though the $V=0$ susceptibility is divergent, long-range order starts building up only for $V\geq 2t$. Our numerical results indicate that long-range order exists for any value of $U>0$, although substantially reduced from the mean-field-theory predictions. We have also studied the character of the transition at zero coupling using finite-size scaling, and concluded that the mean-field-theory predictions are essentially correct except for a prefactor, as occurs in one dimension.

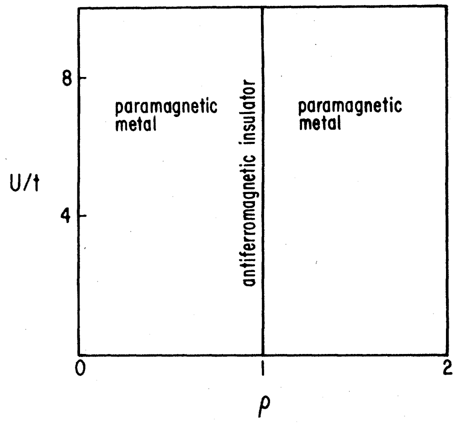

FIG. 23. Conjectured ground-state phase diagram for the two-dimensional Hubbard model.

For the non-half-filled band, although we have only explored a few points on the phase diagram, we believe our results strongly suggest that no long-range magnetic order exists. We have also found no indication of even short-ranged ferromagnetic correlations. Concerning this last point, our findings are in agreement with those of other authors,[10] who suggested that bipartite lattices are particularly unfavorable for ferromagnetic correlations.

Unfortunately, our phase diagram, Fig. 23, is much less interesting than the Hartree-Fock phase diagram, Fig. 3. It appears that an approximate (and qualitatively wrong) solution to a simple model does much better in describing features of real materials than the exact solution of the model. In fact, our model does not really describe itinerant magnetism: only for the insulating case do we find magnetic long-range order. Although this could be due to dimensionality (work on the three-dimensional Hubbard model is in progress), it is possible that a model to describe itinerant magnetism will have to necessarily include band degeneracy.

We have also explored pairing correlations and, in particular, triplet pairing. Recently, it has been suggested that triplet superconductivity could occur in strongly interacting fermion systems, driven by an electronic interaction mechanism.[29] Our results suggest that this is unlikely in a single-band model; it could, however, conceivably occur in models with more than one band.

Several questions about the two-dimensional Hubbard model remain open. The consequences of the singularity in the density of states coinciding with the nesting of the Fermi surface should be investigated theoretically beyond the RPA: a renormalization-group treatment appears possible. For strong coupling, the formulation we have